Designing diameter-modulated heterostructure nanowires of PbTe/Te by controlled dewetting

Communication

Designing Diameter-modulated Heterostructure Nanowires of PbTe/Te by Controlled Dewetting

Abinash Kumar, Subhajit Kundu, Debadarshini Samantaray, Paromita Kundu, Daniele Zanaga, Sara Bals, and N. Ravishankar

Nano Lett., **Just Accepted Manuscript** • DOI: 10.1021/acs.nanolett.7b02442 • Publication Date (Web): 29 Nov 2017

Designing Diameter-Modulated Heterostructure Nanowires of PbTe/Te by controlled dewetting

Abinash Kumar,[†‡] Subhajit Kundu,[†‡] Debadarshini Samantaray,[†] Paromita Kundu,[§] Daniele Zanaga,[§] Sara Bals,[§] and N. Ravishankar[†]*

[†] Materials Research Centre, Indian Institute of Science, Bangalore 560012, India

[§] Electron Microscopy for Materials Science (EMAT), University of Antwerp, Groenenborgerlaan 171, B-2020 Antwerp, Belgium

Abstract

Heterostructures consisting of semiconductors with controlled morphology and interfaces find applications in many fields. A range of axial, radial and diameter-modulated nanostructures have been synthesized primarily using vapor phase methods. Here, we present a simple wet chemical routine to synthesize heterostructures of PbTe/Te using Te nanowires as templates. A morphology evolution study for the formation of these heterostructures has been performed. Based on these control experiments, a pathway for the formation of these nanostructures is proposed. Reduction of a Pb precursor to Pb on Te nanowire templates followed by interdiffusion of Pb/Te leads to the formation of a thin shell of PbTe on the Te wires. Controlled dewetting of the thin shell leads to the formation of cube-shaped PbTe that is periodically arranged on the Te wires. Using control experiments, we show that different reactions parameters like rate of addition of the reducing agent, concentration of Pb precursor and thickness of initial Te nanowire play a critical role in controlling the spacing between the PbTe cubes on the Te wires. Using simple surface energy arguments, we propose a mechanism for the formation of the hybrid. The principles presented are general and can be exploited for the synthesis of other nanoscale heterostructures.

Keywords: Heterostructures, Te, PbTe, diameter-modulated, dewetting, STEM-XEDS tomography

Tellurium-based nanomaterials have made a great impact in different areas like energy, optoelectronics and memory storage. For example, lead telluride, bismuth telluride, antimony telluride and their solid solutions have shown remarkable thermoelectric conversion efficiencies at low/ambient temperatures.[1-8] Germanium and antimony telluride alloys show reversible crystalline and amorphous phase transformations that qualify them as phase-change materials for data storage applications.[9-12] Cadmium telluride, zinc telluride and their solid solutions are used for optoelectronic applications.[13-16] Recently, lead telluride (PbTe) has attracted a lot of attention in the field of thermoelectrics and optoelectronics due to its low band gap (0.31 eV at 300 K) and large excitonic Bohr radius (~46 nm).[17] Various nanostructures such as nanoparticles,[18, 19] nanowires,[17, 20-22] nanotubes[23, 24] and nanoplates[18] have been synthesized to enhance the figure of merit. PbTe has face-centered cubic crystal structure that does not readily form 1D nanostructures; various mechanisms of symmetry breaking during growth of high symmetry crystals leading to 1D structures have been discussed in the literature.[25, 26] Band structure engineering using thallium impurity levels in PbTe results in an increase in ZT value to 1.5 at 773 K.[27] PbTe QDs based solar cells have shown a remarkable increase in external quantum efficiency above 120% due to increase in multiple exciton generation (MEG).[28]

Heterostructures of different nanomaterials have shown to greatly enhance material properties as compared to their constituents. For example, PbO/TiO_2 and CdS/ZnO show higher photocatalytic activity as compared to TiO_2 or ZnO.[29, 30] Different types of heterostructures with different geometries have been synthesized using a variety of methods.[31-47] Most of these are based on vapor-phase/thin film routes like molecular beam epitaxy,[48] or chemical vapor deposition methods[49, 50] while some are based on solution-based approaches.[29, 30, 51-53] Heterostructures synthesized using solution-based approach have the advantages of relatively

lower cost and are thus scalable. Recently, synthesis of periodically spaced nanoparticles on nanowires has been explored using chemical vapor method in Si-Ge and Ga_2O_3-SnO_2 systems using a novel Plateau-Rayleigh crystal growth.[49, 50, 54] Here, we present a wet chemical method to synthesize PbTe on Te nanowires and trace its evolution into beaded PbTe nanowires. We demonstrate that different reaction parameters like rate of addition of reducing agent, concentration of Pb precursor and diameter of Te nanowire template play an important role in controlling the bead spacing on these nanowires. The mechanism of formation of these heterostructures is presented.

Te nanowires have been synthesized using a rapid, microwave-based method which is a modified literature method (Supporting information, Experimental Section).[55] X-ray diffraction (XRD) pattern of the as-synthesized Te nanowires (**Figure S1)** show peaks corresponding to the rhombohedral phase (cell constants as a = 0.4457 nm and c = 0.5927 nm) which is in good agreement with standard literature (JCPDS Card No.- 36-1452). Bright-field TEM imaging (**Figure 1a**) shows that the Te nanowires have a smooth surface and a distribution of diameters from 20 to 120 nm. Selected-area electron diffraction from an isolated Te nanowire (**Inset of Figure 1a**) shows a single set of spots corresponding to the $[\bar{1}100]$ zone axis of rhombohedral phase of Te indicating that the nanowires are single crystalline in nature.

PbTe nanowires were synthesized using the Te nanowires as a template. In a typical synthesis, $PbAc_2$ was added to the PVP-capped Te nanowire solution and the resultant solution was heated to 120 °C. 3 ml of hydrazine hydrate was added to this solution to reduce the lead salt, in 100 µl installments every 3 mins. The XRD pattern acquired from the final product (PTNW3) after 3 ml addition of hydrazine (**Figure S2**) shows peaks corresponding to the rock-salt PbTe phase with a lattice constant of a = 0.646 nm (JCPDS Card No.- 77-0246) with no discernible peaks from the

Te phase. **Figure 1b** shows a typical low magnification SEM image of the as-synthesized product showing the presence of discrete beads on the surface of the wires. Imaging the beaded nanowire at a higher magnification in the SEM (**Inset of Figure 1b**) reveals that the beads are faceted. **Figure 1c** is a bright-field TEM image of the as-synthesized beaded PbTe nanowires where the beads are arranged in a periodic manner on the nanowire. Statistical analysis based on TEM images show that the beads have an average pitch (spacing between consecutive beads) of 109 ± 25 nm, amplitude (size of each bead) of 110 ± 18 nm and diameter (of spacer region between beads) of 58 ± 7 nm. Selected-area electron diffraction from an isolated nanowire (**Inset of Figure 1c**) show a single set of spots corresponding to the $[1\bar{1}0]$ zone axis of cubic PbTe phase indicating that the nanowires are single crystalline in nature. **Figure 1d** shows the high-resolution TEM image from such a nanowire showing fringes corresponding to (111) and (200) plane of PbTe and indicating [111] as growth direction of the nanowires. The formation of a thin amorphous layer at the surface is observed upon prolonged exposure of the sample by the electron beam, possibly due to the formation of oxide of lead or tellurium.

To get further insight into the morphology and elemental composition of the beaded nanostructures, imaging and energy dispersive X-ray spectroscopy (EDXS) has been carried out in STEM mode. **Figure 1e** shows a high magnification (high-angle annular dark field scanning transmission electron microscope) HAADF-STEM image in which faceted structures can be seen in projection. A region of lighter contrast could be traced inside the nanowires that could be due to the presence of unreacted Te or voids. STEM-EDXS analysis (**Figure 1f-i**) shows that such a contrast is due to the presence of a small amount of Te that could not be detected in XRD. Point EDXS from several beads shows that beads in this beaded structure are stoichiometric having 1:1 (Pb:Te) composition (**Figure S18**).

In the above characterization, we obtained partial morphological and elemental distribution information from 2D projection images; obtaining 3D information provides more insights into growth and mechanisms.[56] For a detailed 3D investigation of the structure of one of such beaded PbTe nanowires sample and their chemical composition, we performed STEM-EDXS tomography, according to the method described in the literature.[57] For STEM and EDXS tomography, tilt series ranging between -70° and +70°, are obtained with images acquired at every 2° and 10°, respectively. In order to obtain the chemically quantified reconstructions, EDXS maps are first quantified in Bruker Esprit through the Cliff-Lorimer method implemented by the software. The quantified maps are then combined with the thickness information obtained from the HAADF-STEM tomography reconstruction, enabling the 3D reconstruction of the elemental distributions. A detailed explanation of the procedure can be found in ref.[57] The 3D reconstructions (3D visualization of STEM tomography volume reconstruction, **Supporting video 1**) show the closely spaced cube shaped PbTe on Te wire template. **Figure 2a & b** show the HAADF-STEM image and volume rendering, respectively, indicating the cubic morphology of PbTe formed around the Te wire template. Interestingly, we observed presence of depressions at different locations on the surface. Upon further investigation, these were identified as funnel-shaped holes/cavities on the PbTe surface, as well as close to the template core with some channels originating from them. The Z-contrast in the orthoslices, presented in **Figure 2c** clearly reveal the distribution of Pb and Te where the darker region at the core possibly represents the presence of unreacted Te and the brighter regions corresponds to PbTe. The presence of funnel-shaped cavities/holes at the PbTe surface and trapped closer to the Te core are further evident from the orthoslices. These lead to channels which terminate either inside or at the exterior surface of the PbTe cubes as seen in the volume renderings and the orthoslices. Details about the

chemical composition are further obtained from EDXS tomography, volume renderings are presented in **Figure 2d-f** showing the presence of Pb in the cubes, however, Te is more uniformly distributed and an unreacted portion remains in the core. The distribution of Pb and Te is more clearly visible in the orthoslices corresponding to Pb (**Figure 2g**) and Te (**Figure 2h**) where Pb is absent at the core. This 3D elemental composition characterization confirms the presence of PbTe cubes on the unreacted Te nanowire core (3D visualization of EDXS tomography volume reconstruction, **Supporting video 2**).

To understand the role of rate of addition of the reducing agent (hydrazine) in controlling the formation of the beads on the Te nanowire template, experiments were carried out with different rates of addition of hydrazine, keeping the total amount of hydrazine addition fixed as 3 ml, the amount added per installment as 100 µl and the total time of heating as 3 hours and only varying the time interval between successive additions of 100 µl. As an extreme case, all the hydrazine hydrate was added in a single installment in one of the experiments. The different conditions used are listed in the experimental section. **Figure 3a-d** show the representative TEM images from these experiments. Electron diffraction and EDS confirmed the formation of the stochiometric PbTe phase in all the cases. However, as the rate of addition is increased, the pitch of the beads decreases (**Figure 3e & S3**). In the extreme case of addition of hydrazine in a single installment, we do not observe the formation of discrete beads on the surface but observe an increased roughness on the product nanowires as compared to the starting Te nanowires. The size of beads (amplitude) does not vary significantly with change in rate of addition of the reducing agent (**Figure S4**). These observations clearly demonstrate that the rate of addition of the reducing agent plays an important role in the morphology development.

To understand the mechanism of formation of the beaded structure, aliquots were collected after 2 min of addition of each installment of the reducing agent to monitor the changes in morphology and phase (**Figure 4a-e & S5**). During the early stage (~ 5 min of reaction after addition of 2nd installment of the reducing agent), it was observed that the surface of the nanowires is still smooth. Electron diffraction showed the presence of rhombohedral Te phase with no signature of PbTe. Randomly shaped aggregates, that were extremely unstable under the electron beam, could be observed on the TEM support membrane and also clinging to the Te wires in some locations (**Figure S7**) that is possibly the unreacted precursor of Pb whose reduction is limited by amount of the reducing agent added at that point of the reaction. As the reaction progresses (after 8 min or after adding the third installment of hydrazine), small undulations are seen on the surface of the nanowires. Electron diffraction at this stage shows the presence of the cubic PbTe phase. After 17 min (after addition of 6th installment of hydrazine), such undulations present on the surface take a distorted cubic shape as can be observed from the TEM image (**Figure 4c**). As the reaction progresses further (after 29 min or after adding 10th installment of hydrazine), the beads grow in size and adopt the facetted cube shape. After 3 hours, beaded PbTe nanowires were formed as illustrated in **Figure 1c**. Statistical analysis (**Figure 4f & S6**) from the obtained TEM and SEM images over extended time (from 30 min to 3 h) shows that pitch and amplitude decrease with reaction time till 3 hours. Upon further heating of these nanowires for 48 hours, no further change in pitch and amplitude has been observed.

Based on the above observations, a possible mechanism for the formation of beaded PbTe nanowires could be proposed. Addition of $PbAc_2$ to the PVP-capped Te nanowire solution leads to adsorption of Pb^{2+} to the surface of the Te nanowires. Such role of PVP as adsorbing agent is

well known in literature.[17, 20] On heating the reaction mixture and adding hydrazine, gradual reduction of Pb^{2+} to Pb on surface of the Te nanowires takes place according to the reaction:

$$Pb^{2+} + 2e^- \rightarrow Pb \quad (-0.1262\ V)$$

$$N_2H_4 \cdot H_2O + 4OH^- \rightarrow N_2 + 5H_2O + 4e^- \quad (1.15\ V)$$

$$2Pb^{2+} + N_2H_4 \cdot H_2O + 4\ OH^- \rightarrow 2Pb + N_2 + 5H_2O$$

$$\Delta G_{red} = -(-2 \times (0.1262+1.15))\ F = -135.33\ kJ/mol$$

G_{red} has a negative value which imply that this reduction reaction is highly feasible.

The Pb atoms thus formed, subsequently diffuse into the Te nanowires, forming PbTe according to the reaction:

$$Pb + Te \rightarrow PbTe\ (G_f = -69.5\ kJ/mol)$$

G_f has also negative value implying that the formation of PbTe is highly feasible.

$$G_{total} = -(135.33 + 69.5) = -204.83\ kJ/mol$$

Thermodynamic calculations indicate that such reactions are indeed feasible. Interdiffusion between Pb and Te leads to the formation of PbTe on the Te nanowire. Here, diffusion of Pb into Te is the dominant mechanism over Te diffusing into Pb. This is because if Te diffusion into Pb is faster than Pb diffusion into Te to form PbTe film, then it would lead to formation of voids in the core of the nanowire which in the extreme case could lead to the formation of a PbTe nanotube. If Pb diffusion into Te nanowires is faster than Te diffusion into Pb, solid nanowire of PbTe without any voids in the core of the nanowire should be observed. As no voids in the core of the nanowire is observed, it can be concluded that the dominant mechanism is by diffusion of Pb into Te rather than Te diffusing into Pb.

One of the key observations from the above experiments is that although the PbTe is located at discrete locations on the nanowire at the end of the reaction, there is no local variation in the

diameter of the remnant Te wire in the regions where the cubes are seen. This observation rules out the nucleation and growth of PbTe locally at these locations. Other possible mechanism like dissolution of initial PbTe film and redeposition into PbTe beads on Te nanowire can be also ruled out. If the initial PbTe film gets dissolved then there should not be any change in the pitch value as the reaction proceed further but a change in pitch value is observed with the reaction time. Also, this mechanism cannot explain the tunability of bead spacing in these nanostructures as observed with changing different reaction parameters.

The fact that the beaded nanowires have uniform diameter Te remnants along them (as observed from several images) suggests that there is a possibility of formation of uniform shell of PbTe on Te nanowire, initially, which eventually dewets to form the beads. Due to faster nature of the process at such reaction condition, no such layer formation is observed at lower reaction time. To capture such a stage, reaction has been performed at lower temperature (60^{o}C) with same addition rate of hydrazine (100 µl per 3 min) which leads to a decrease in the reaction kinetics (**Figure 5e-h & S8**). After 15 min of reaction time, an aliquot is taken out from the reaction mixture and drop-casted on the TEM support membrane and cleaned for microscopy analysis. It is indeed observed that a film forms onto Te nanowires after 15 min of reaction (**Figure 5e & g**). **Figure 5f** shows the EDXS elemental scan from one the 15 min sample reveals that Pb and Te both are present at the surface of the nanowires. After 30 min of reaction time, the film dewets into beads arranged in periodic manner onto the Te nanowires. As reaction progress further to 3 hrs, a periodic arrangement of cube shaped PbTe beads is observed to form onto the Te nanowires (**Figure 5 h**). So, the final product is then formed by a solid state dewetting process of the PbTe on the surface of the Te wires. The beads adopt a well-defined cubic shape with exposure of the lower energy (100) facets of the PbTe structure. Volume rendering of PbTe

cubes (**Figure 2b**) show the presence of cavities inside these cubes which can be formed possibly due to N_2 gas which evolves during the reduction reaction of lead ions with hydrazine hydrate as mentioned above.

The pitch of the dewet beads varies with the rate of addition of the reducing agent whereas no significant variation could be observed in its amplitude. With a higher rate of addition, a larger amount of reduced Pb is available for the formation of initial PbTe leading to the formation of a thicker shell. The variation in the pitch can be understood in terms of the difference in thickness of the initial PbTe that is formed. A higher rate of addition leads to a thicker shell that eventually leads to a closer spacing/pitch between the beads after dewetting. It is well known from the studies on thin film dewetting that higher precursor flux leads to shorter surface diffusion length of atoms which in this case gives rise to closely spaced beads.[58] Slower rate of addition of the reducing agent leads to low supersaturation of Pb atoms during incubation time (time when the initial PbTe film is formed) that eventually leads to the formation of thinner shell. Thinner shell can dewet with larger diffusion lengths leading to the formation of largely spaced beads. With further addition of reducing agent, it is seen (**Figure 4f & S6**) that the average pitch and the amplitude decrease. This can be explained by the formation of PbTe shells in the exposed Te regions between the beads that further dewets to smaller beads leading to a reduction in both the pitch and the amplitude.

To further validate the role of supersaturation in the variation of pitch, experiments with varying concentration of lead precursor with fixed addition rate of hydrazine hydrate (100 µl per 3 min) have been performed. As the amount of Pb precursor is doubled (as compared to the PTNW3 experiment, 1:1 Pb:Te precursor ratio), non-beaded PbTe/Te nanowires are formed (**Figure 5a**). This is very similar to the case of addition of hydrazine hydrate in a single

instalment. While at the opposite extreme, when the amount of Pb precursor is decreased to half of that in sample PTNW3, beads with a higher spacing is observed (**Figure 5b**). This clearly indicates that a lower supersaturation of the Pb precursor leads to thinner films dewetting into beads with higher spacing. The opposite case of higher supersaturation (at higher concentration) leads to thicker films which do not dewet leading to non-beaded (or smooth) nanowire. Similarly, a variation in diameter of parent Te nanowire will also lead to variation in thickness of initial PbTe film formed. A thicker parent Te nanowire will lead to thinner PbTe film than thinner parent Te nanowire (calculation has been shown in supporting information). So, thicker parent Te nanowire will give rise to nanowire with higher bead spacing as observed experimentally (**Figure 5 c & d**).

In order to eliminate the effects of multiple additions of the reducing agent on the final microstructure, a reaction was carried out with only 50 µl addition of the reducing agent (hydrazine). Since the quantity of reducing agent is significantly reduced in this case, only a very small amount of Pb is reduced leading to the formation of a very thin shell that eventually leads to very widely spaced PbTe beads. It was not possible to retain the thin shell structure by quenching indicating that the kinetics of dewetting is rapid. Due to the inhomogeneity arising from the limited supply of the reducing agent, the microstructure is very inhomogeneous in this case (**Figure S9a**). HRTEM confirmed the presence of Te nanowires in between two beads in these nanowires (**Figure S9b**). With an increase in amount of hydrazine (100 µl), the pitch value decreases. It has been also observed that the cylindrical spacer present in between two consecutive beads is only Te nanowire (**Figure S10a**). With further increase in amount of hydrazine to 200 µl, the pitch value decreases further but here the cylindrical spacer contains a shell of PbTe on the Te nanowires (**Figure S10b**).

The dewetting process is one where a shell of materials breaks up into an array of particles.[59] A simplified geometrical analysis (Supporting Information) based on surface energy has been performed to compare the energies of the starting and ending stated to rationalize the formation of the beaded structure by dewetting. It is assumed in the model that a cylinder of certain size breaks completely into cubical shape beads neglecting the cylindrical spacer regions in between. In this model, interfacial energy between Te and PbTe has been neglected based on our observation that the regions between the beads having a PbTe/Te interface remains intact even after 48 hours of reaction indicating that this interface is not unfavorable under these reaction conditions. Using the constraint of volume conservation leads to a prediction that the pitch is inversely proportional to the radius of cylinder if the size of bead formed is assumed to be constant (**Figure S11**). This inverse proportionality relation validates the trends seen in our experimental observations that clearly show that a larger shell thickness of PbTe leads to a closer spacing between the particles.

The ratio of the total surface energy of a beaded structure and the cylindrical smooth nanowire of PbTe is calculated and found to depend on both the radius of cylinder (thickness of the film) and spacing of beads (pitch). Formation of beaded structures will be only favorable if beaded structure has lower surface energy as compared to the smooth nanowire. Thus, the ratio of surface energy of beaded and smooth nanowire should be less than one for certain pitch value for a constant radius of cylinder. We have found that there exists a minimum value of pitch for a constant radius of cylinder where the ratio become one. This minimum pitch that favors dewetting also increases with the radius of the cylinder (thickness of the film) (**Figure S12**). While volume conservation leads to a decrease in the pitch with increase in thickness, it is clear that beyond a certain thickness, dewetting will be suppressed as this pitch will become smaller

than what is required by energy considerations. Thus, in the case of sample where the reducing agent is added in a single installment or the ratio of Pb and Te precursor become double, a thick shell of PbTe forms that remains stable against dewetting. One of the questions that remains is that dewetting is seen to take place on the Te wires at the initial stages while at later stages, a shell of PbTe remains in between the dewet cubes. This can be understood in terms of the above-mentioned result. This can also be understood in terms of the minimum pitch requirements for dewetting in terms of the energy considerations. If the spacing between the already dewet particles is smaller than the required pitch, then the film will be stable.

The growth mechanism of beaded PbTe nanowires in our case follow the recently proposed Plateau-Rayleigh (P-R) crystal growth model demonstrated for Si/Ge on Si in a typical gas phase reaction.[49] These beaded structures also give rise to modulations in diameter along the length of PbTe nanowires. Such diameter modulations are highly tunable in terms of spacing which indicates that this phenomenon is clearly different from that of P-R instabilities. It has been found that by introducing modulations in diameter of Si nanowires, optical absorption got enhanced over a broad spectral range and also these show lower value of thermal conductivity due to enhancement in phonon scattering.[60, 61] These modulations were introduced using a vapor-phase process but here we are able to introduce modulations using wet chemical method. Developing an understanding of formation mechanism of these modulations in PbTe will open a door to synthesize diameter-modulated nanowires of different materials. In future, introducing diameter-modulations in nanowires will lead to a dramatic increase in properties of nanomaterials that can be used for device fabrication for different applications.

ASSOCIATED CONTENT

Supporting Information

XRD data, statistical analysis, additional TEM images and geometrical analysis.

Supporting Video 1

Supporting Video 2

AUTHOR INFORMATION

Corresponding Author

*E-mail: nravi@iisc.ac.in; raviisc@gmail.com

Author Contributions

‡ These authors contributed equally.

Funding Sources

SERB, Department of Science and Technology (DST), Government of India

Notes

The authors declare no competing financial interest.

ACKNOWLEDGMENT

NR acknowledges financial support from SERB, DST, Government of India. The authors acknowledge the electron microscopy facilities at the Advanced Facility for Microscopy and Microanalysis, IISc. SB, PK and DZ acknowledge ERC Starting Grant #335078 COLOURATOMS for financial support.

REFERENCES

1. Dughaish, Z. H. *Physica B: Condensed Matter* **2002,** *322*, 205-223.
2. Heremans, J. P.; Thrush, C. M.; Morelli, D. T. *Phy. Rev. B* **2004,** *70*, 115334.
3. Poudel, B.; Hao, Q.; Ma, Y.; Lan, Y.; Minnich, A.; Yu, B.; Yan, X.; Wang, D.; Muto, A.; Vashaee, D.; Chen, X.; Liu, J.; Dresselhaus, M. S.; Chen, G.; Ren, Z. *Science* **2008,** *320*, 634-638.
4. Venkatasubramanian, R.; Siivola, E.; Colpitts, T.; O'Quinn, B. *Nature* **2001,** *413*, 597-602.
5. Yamashita, O.; Tomiyoshi, S.; Makita, K. *J. Appl. Phys.* **2003,** *93*, 368-374.
6. Zhou, J.; Jin, C.; Seol, J. H.; Li, X.; Shi, L. *Appl. Phys. Lett.* **2005,** *87*, 133109.
7. Zhang, G.; Kirk, B.; Jauregui, L. A.; Yang, H.; Xu, X.; Chen, Y. P.; Wu, Y. *Nano Lett.* **2012,** *12*, 56-60.
8. Wang, T.; Mehta, R.; Karthik, C.; Ganesan, P. G.; Singh, B.; Jiang, W.; Ravishankar, N.; Borca-Tasciuc, T.; Ramanath, G. *J. Phys. Chem. C* **2010,** *114*, 1796-1799.
9. Lencer, D.; Salinga, M.; Grabowski, B.; Hickel, T.; Neugebauer, J.; Wuttig, M. *Nat. Mater.* **2008,** *7*, 972-977.
10. Lee, S.-H.; Jung, Y.; Agarwal, R. *Nat. Nano.* **2007,** *2*, 626-630.
11. Sun, X.; Yu, B.; Ng, G.; Meyyappan, M. *J. Phys. Chem. C* **2007,** *111*, 2421-2425.
12. Raoux, S.; Wełnic, W.; Ielmini, D. *Chem. Rev.* **2010,** *110*, 240-267.
13. Xie, X.; Kwok, S.-Y.; Lu, Z.; Liu, Y.; Cao, Y.; Luo, L.; Zapien, J. A.; Bello, I.; Lee, C.-S.; Lee, S.-T.; Zhang, W. *Nanoscale* **2012,** *4*, 2914-2919.
14. Tu, C.-C.; Lin, L. Y. *Appl. Phys. Lett.* **2008,** *93*, 163107.
15. Başol, B. M.; McCandless, B. *J. Photon. Energy.* **2014,** *4*, 040996.
16. Kum, M. C.; Jung, H.; Chartuprayoon, N.; Chen, W.; Mulchandani, A.; Myung, N. V. *J. Phys. Chem. C* **2012,** *116*, 9202-9208.
17. Tai, G. a.; Zhou, B.; Guo, W. *J. Phys. Chem. C* **2008,** *112*, 11314-11318.
18. Zhu, T. J.; Chen, X.; Meng, X. Y.; Zhao, X. B.; He, J. *Cryst. Growth Des.* **2010,** *10*, 3727-3731.
19. Ziqubu, N.; Ramasamy, K.; Rajasekhar, P. V. S. R.; Revaprasadu, N.; O'Brien, P. *Chem. Mater.* **2010,** *22*, 3817-3819.
20. Liang, H.-W.; Liu, S.; Wu, Q.-S.; Yu, S.-H. *lnorg. Chem.* **2009,** *48*, 4927-4933.

21. Yang, H.; Finefrock, S. W.; Albarracin Caballero, J. D.; Wu, Y. *J. Am. Chem. Soc.* **2014,** *136*, 10242-10245.
22. Purkayastha, A.; Yan, Q.; Gandhi, D. D.; Li, H.; Pattanaik, G.; Borca-Tasciuc, T.; Ravishankar, N.; Ramanath, G. *Chem. Mater.* **2008,** *20*, 4791-4793.
23. Hu, J.; Chen, Z.; Jiang, H.; Sun, Y.; Bando, Y.; Golberg, D. *J. Mater. Chem.* **2009,** *19*, 3063-3068.
24. Tong, H.; Zhu, Y.-J.; Yang, L.-X.; Li, L.; Zhang, L. *Angew. Chem. Int. Ed.* **2006,** *45*, 7739-7742.
25. Halder, A.; Kundu, P.; Viswanath, B.; Ravishankar, N. *J. Mater. Chem.* **2010,** *20*, 4763-4772.
26. Viswanath, B.; Kundu, P.; Halder, A.; Ravishankar, N. *J. Phys. Chem. C* **2009,** *113*, 16866-16883.
27. Heremans, J. P.; Jovovic, V.; Toberer, E. S.; Saramat, A.; Kurosaki, K.; Charoenphakdee, A.; Yamanaka, S.; Snyder, G. J. *Science* **2008,** *321*, 554-557.
28. Böhm, M. L.; Jellicoe, T. C.; Tabachnyk, M.; Davis, N. J. L. K.; Wisnivesky-Rocca-Rivarola, F.; Ducati, C.; Ehrler, B.; Bakulin, A. A.; Greenham, N. C. *Nano Lett.* **2015,** *15*, 7987-7993.
29. Leelavathi, A.; Mukherjee, B.; Nethravathi, C.; Kundu, S.; Dhivya, M.; Ravishankar, N.; Madras, G. *RSC Adv.* **2013,** *3*, 20970-20977.
30. Kundu, P.; Deshpande, P. A.; Madras, G.; Ravishankar, N. *J. Mater. Chem.* **2011,** *21*, 4209-4216.
31. Wang, D.; Xin, H. L.; Hovden, R.; Wang, H.; Yu, Y.; Muller, D. A.; DiSalvo, F. J.; Abruña, H. D. *Nat. Mater.* **2013,** *12*, 81-87.
32. Tao, F.; Grass, M. E.; Zhang, Y.; Butcher, D. R.; Renzas, J. R.; Liu, Z.; Chung, J. Y.; Mun, B. S.; Salmeron, M.; Somorjai, G. A. *Science* **2008,** *322*, 932-934.
33. Zhong, C. J.; Maye, M. M. *Adv. Mater.* **2001,** *13*, 1507-1511.
34. Bu, L.; Zhang, N.; Guo, S.; Zhang, X.; Li, J.; Yao, J.; Wu, T.; Lu, G.; Ma, J.-Y.; Su, D.; Huang, X. *Science* **2016,** *354*, 1410-1414.
35. Huang, X.; Tang, S.; Liu, B.; Ren, B.; Zheng, N. *Adv. Mater.* **2011,** *23*, 3420-3425.
36. Zhao, Z.; Liu, J.; Cui, F.; Feng, H.; Zhang, L. *J. Mater. Chem.* **2012,** *22*, 9052-9057.
37. Lauhon, L. J.; Gudiksen, M. S.; Wang, D.; Lieber, C. M. *Nature* **2002,** *420*, 57-61.

38. Tang, J.; Huo, Z.; Brittman, S.; Gao, H.; Yang, P. *Nat. Nano.* **2011,** *6*, 568-572.
39. Hu, M.; Giapis, K. P.; Goicochea, J. V.; Zhang, X.; Poulikakos, D. *Nano Lett.* **2011,** *11*, 618-623.
40. Su, Y.; Wei, X.; Peng, F.; Zhong, Y.; Lu, Y.; Su, S.; Xu, T.; Lee, S.-T.; He, Y. *Nano Lett.* **2012,** *12*, 1845-1850.
41. Zou, X.; Wang, J.; Liu, X.; Wang, C.; Jiang, Y.; Wang, Y.; Xiao, X.; Ho, J. C.; Li, J.; Jiang, C.; Fang, Y.; Liu, W.; Liao, L. *Nano Lett.* **2013,** *13*, 3287-3292.
42. Chen, D.; Yin, L.; Ge, L.; Fan, B.; Zhang, R.; Sun, J.; Shao, G. *Sens. Actuators B* **2013,** *185*, 445-455.
43. Sofianou, M.-V.; Boukos, N.; Vaimakis, T.; Trapalis, C. *Appl. Catal. B: Environ.* **2014,** *158–159*, 91-95.
44. Fei, F.; Wei, Z.; Wang, Q.; Lu, P.; Wang, S.; Qin, Y.; Pan, D.; Zhao, B.; Wang, X.; Sun, J.; Wang, X.; Wang, P.; Wan, J.; Zhou, J.; Han, M.; Song, F.; Wang, B.; Wang, G. *Nano Lett.* **2015,** *15*, 5905-5911.
45. Li, Y.; Zhang, J.; Zheng, G.; Sun, Y.; Hong, S. S.; Xiong, F.; Wang, S.; Lee, H. R.; Cui, Y. *ACS Nano* **2015,** *9*, 10916-10921.
46. Fang, H.; Feng, T.; Yang, H.; Ruan, X.; Wu, Y. *Nano Lett.* **2013,** *13*, 2058-2063.
47. Fang, H.; Yang, H.; Wu, Y. *Chem. Mater.* **2014,** *26*, 3322-3327.
48. Farag, A. A. M.; Yahia, I. S.; Wojtowicz, T.; Karczewski, G. *J. Phys. D: Appl. Phys.* **2010,** *43*, 215102.
49. Day, R. W.; Mankin, M. N.; Gao, R.; No, Y.-S.; Kim, S.-K.; Bell, D. C.; Park, H.-G.; Lieber, C. M. *Nat. Nano.* **2015,** *10*, 345-352.
50. Alonso-Orts, M.; Sánchez, A. M.; Hindmarsh, S. A.; López, I.; Nogales, E.; Piqueras, J.; Méndez, B. *Nano Lett.* **2017,** *17*, 515-522.
51. Kundu, P.; Halder, A.; Viswanath, B.; Kundu, D.; Ramanath, G.; Ravishankar, N. *J. Am. Chem. Soc.* **2010,** *132*, 20-21.
52. Kundu, S.; Ravishankar, N. *Nanoscale* **2016,** *8*, 1462-1469.
53. Kundu, S.; Kundu, P.; Tendeloo, G. V.; Ravishankar, N. *Small* **2014,** *10*, 3895-3900.
54. Day, R. W.; Mankin, M. N.; Lieber, C. M. *Nano Lett.* **2016,** *16*, 2830-2836.
55. Li, Z.; Zheng, S.; Zhang, Y.; Teng, R.; Huang, T.; Chen, C.; Lu, G. *J. Mater. Chem. A* **2013,** *1*, 15046-15052.

56. Kundu, P.; Heidari, H.; Bals, S.; Ravishankar, N.; Van Tendeloo, G. *Angew. Chem. Int. Ed.* **2014,** *53*, 3970-3974.

57. Zanaga, D.; Altantzis, T.; Polavarapu, L.; Liz-Marzán, L. M.; Freitag, B.; Bals, S. *Part. Part. Syst. Charact.* **2016,** *33*, 396-403.

58. Smith, D. L., *Thin-Film Deposition: Principles and Practice*. McGraw-Hill Education:New York, 1995.

59. Basu, J.; Carter, C. B.; Divakar, R.; Mukherjee, B.; Ravishankar, N. *Appl. Phys. Lett.* **2009,** *94*, 171114.

60. Ko, M.; Baek, S.-H.; Song, B.; Kang, J.-W.; Kim, S.-A.; Cho, C.-H. *Adv. Mater.* **2016,** *28*, 2504-2510.

61. Jeremie, M.; Masahiro, N. *Jpn. J. Appl. Phys.* **2014,** *53*, 06JE09.

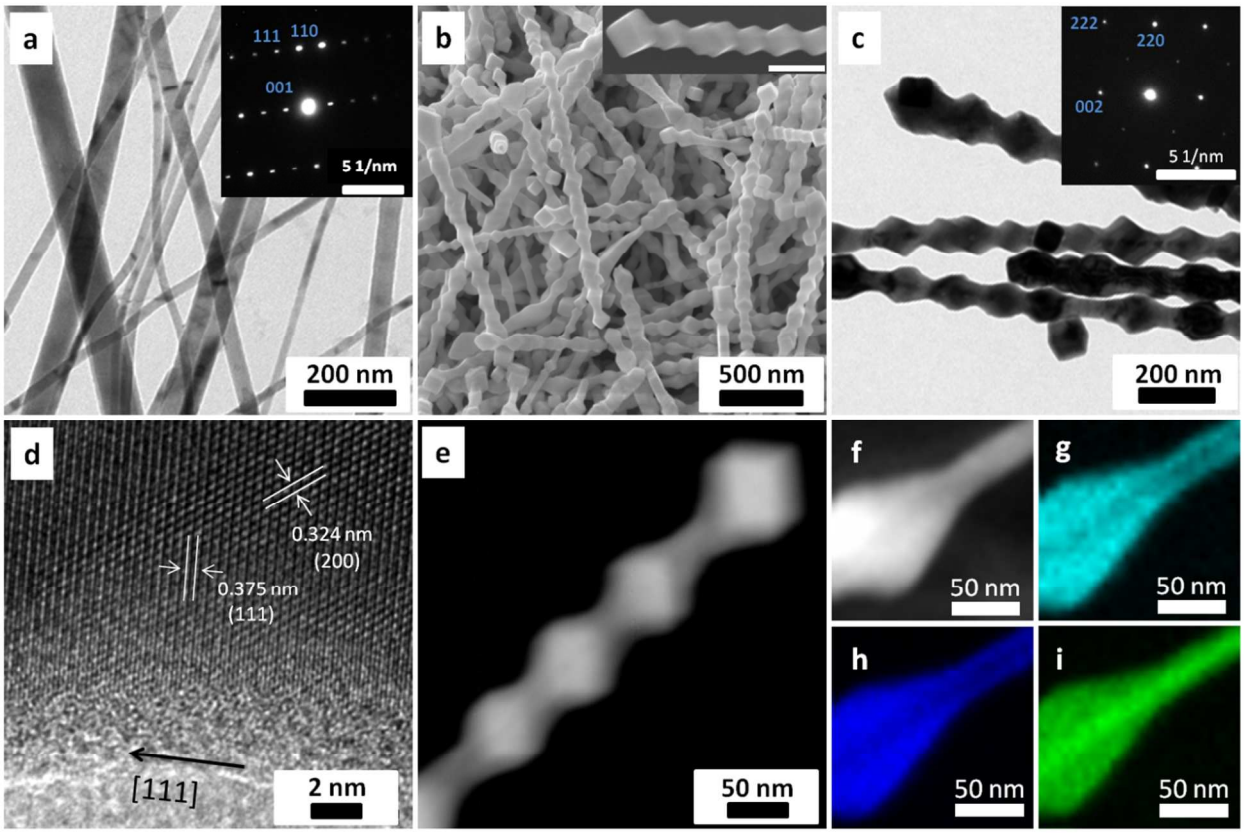

Figure 1. (a) Bright-field TEM image of Te nanowires, Inset: SAED pattern from Te nanowire, (b) Low magnification FESEM image of PbTe nanowires (PTNW3), Inset: High magnification FESEM image of PbTe nanowire, Scale bar, 200 nm, (c) Bright-field TEM image of PbTe nanowires, Inset: SAED pattern from PbTe nanowire, (d) High-resolution TEM of PbTe nanowire, (e) HAADF-STEM image of PbTe Nanowire, (f) HAADF-STEM image of selected area for EDXS elemental map, (g) Pb-L, (h) Pb-M and (i) Te-L are EDXS elemental maps of PbTe nanowires respectively.

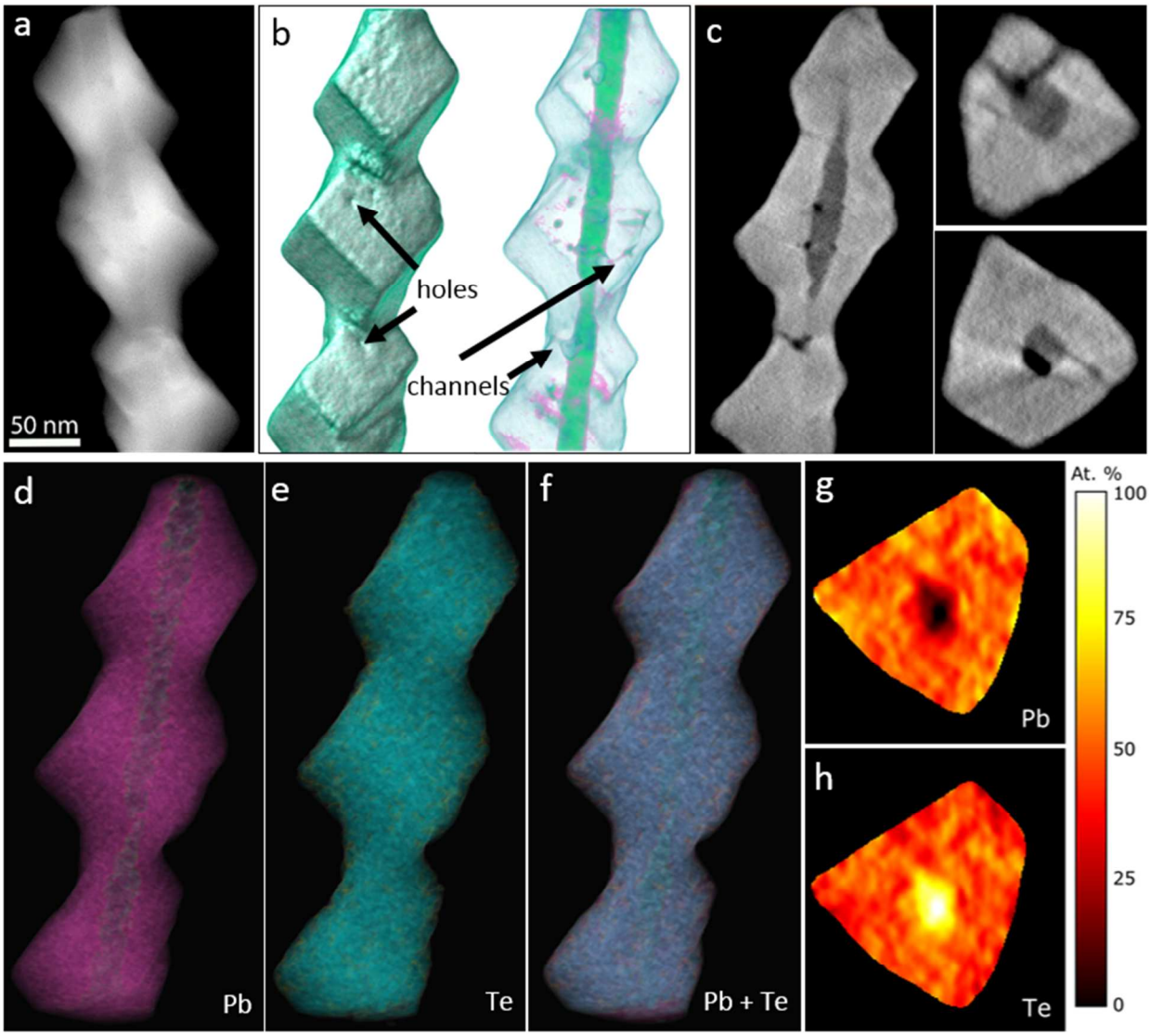

Figure 2. Electron tomography results of beaded PbTe nanowires are shown here where, (a) shows the HAADF-STEM image of a typical PbTe nanowire. (b) shows volume renderings obtained from HAADF-STEM tomography where false color and different visualization conditions are used to indicate the presence of funnel-shaped holes/cavities and the channels originating from them (marked in the figure). (c) orthoslices from the HAADF-STEM reconstruction, giving an overview of the structure, confirming the presence of cavities closer to the Te core which lead to channels either terminating inside or opening at the surface of the cubes. Volume rendering obtained from EDXS tomography are given in (d-f) showing the elemental distribution of Pb and Te. (g) and (h) shows orthoslices for Pb and Te, respectively, highlighting the presence of a pure Te wire in the center and PbTe beads around.

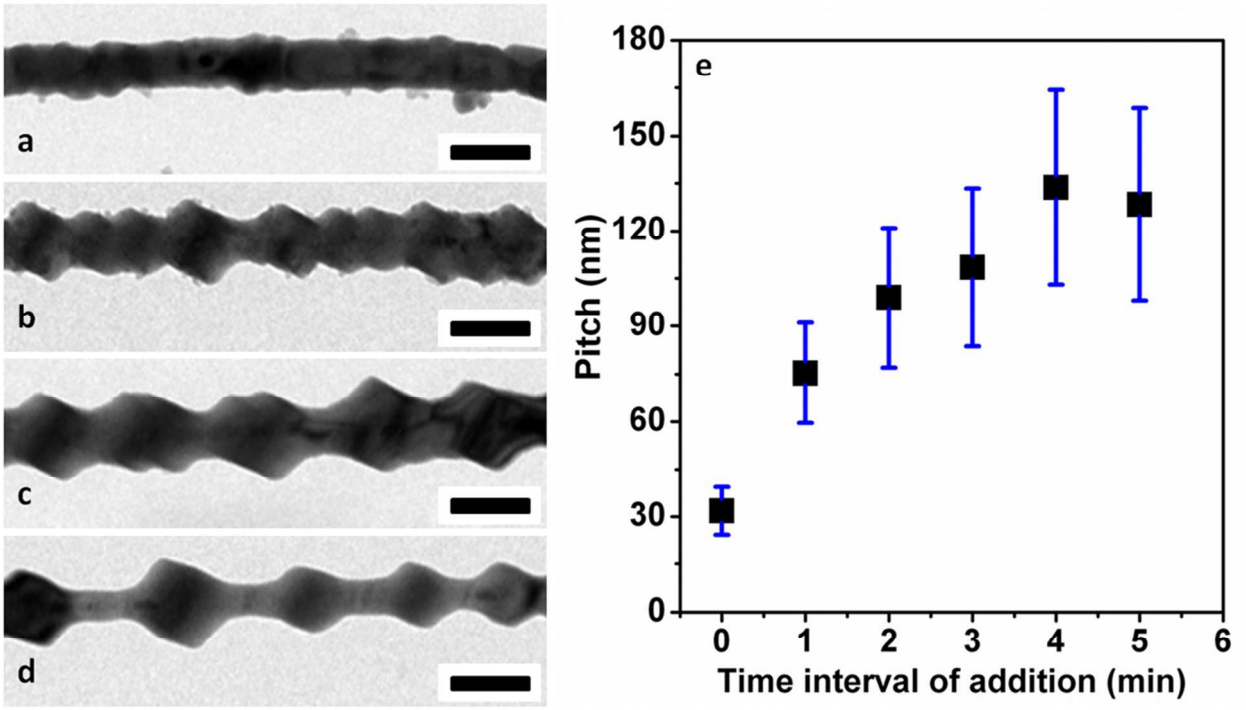

Figure 3. Bright-field TEM images of PbTe nanowires synthesized by adding hydrazine hydrate (HH) at different rates, (a) 3 ml of HH is added in a single installment, 3 ml of HH is added in 0.1 ml installments at different time intervals (b) 1 min (c) 3 min and (d) 5 min respectively. Scale bars: 100 nm. (e) Variation of pitch in different samples synthesized by adding HH in installments at different time intervals.

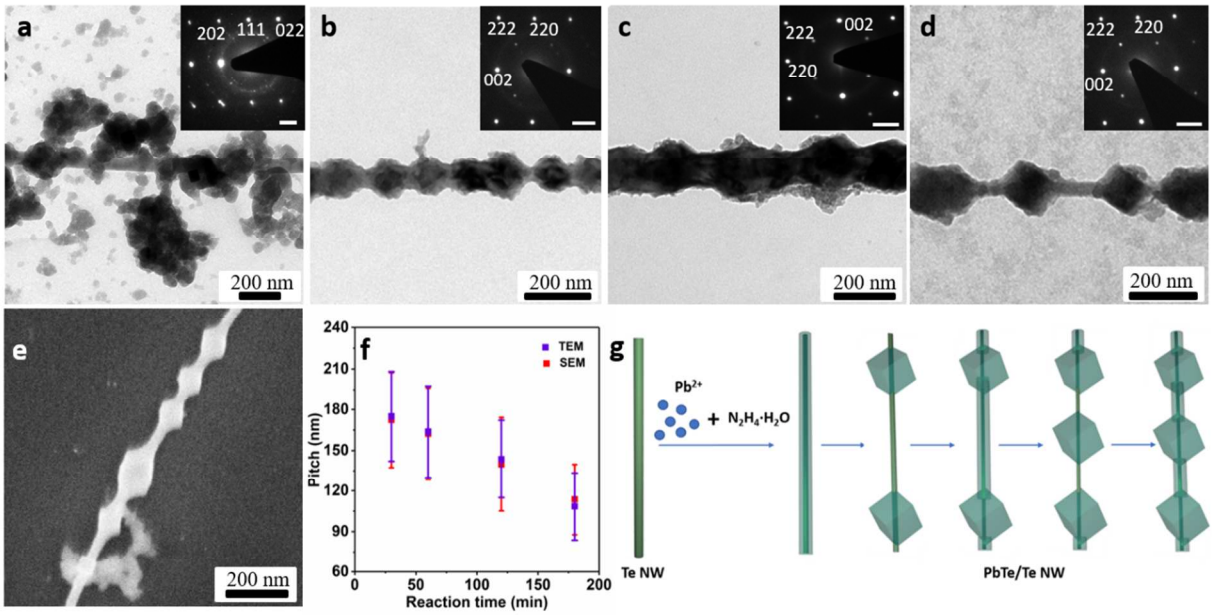

Figure 4. Morphology evolution of beaded PbTe nanowires at different reaction time: (a) 5 min (b) 8 min (c) 17 min and (d) 30 min respectively. Inset shows the corresponding selected-area electron diffraction from the respective samples (Scale bar, 5 1/nm). (e) SEM image of PbTe nanowire after 30 min of the reaction. (f) Variation of Pitch of beads with reaction time. (g) Schematic showing the mechanism of transformation of Te nanowires to beaded PbTe nanowires, as observed experimentally.

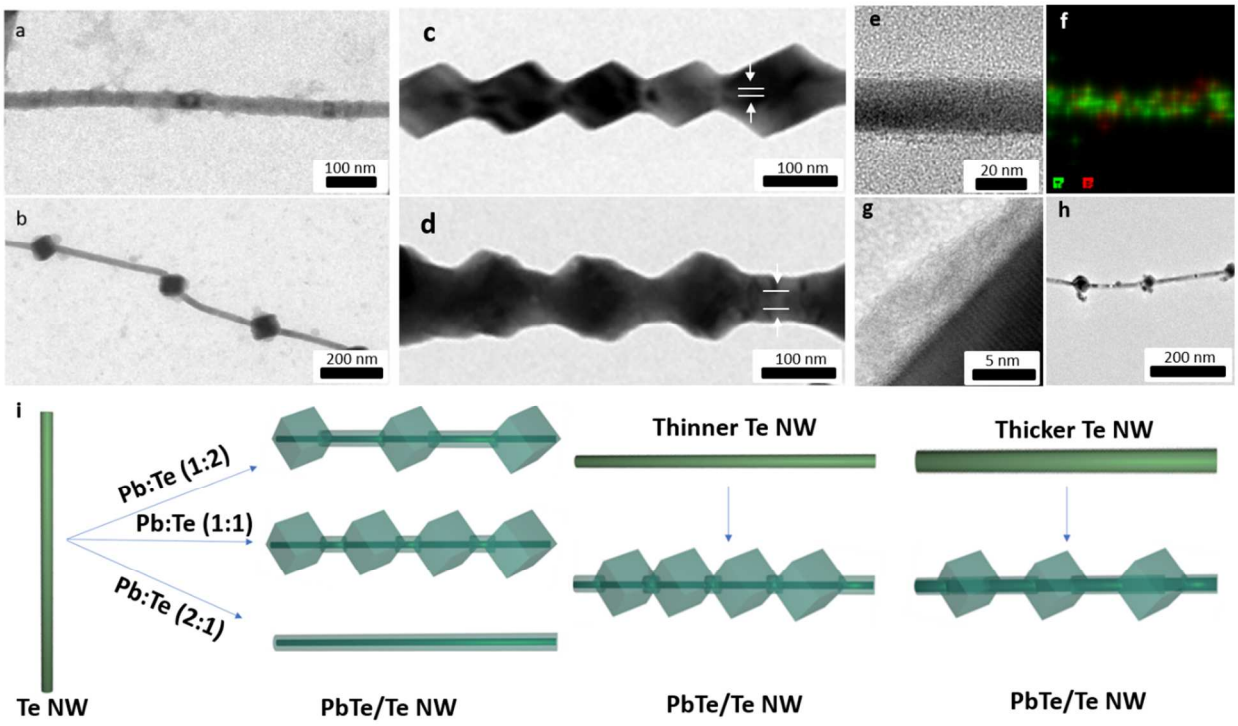

Figure 5. Bright field TEM images of PbTe nanowires using different concentration of Pb precursor: (a) 2:1 (Pb:Te) & (b) 1:2 (Pb:Te) respectively. (c) & (d) Bright field TEM images of beaded PbTe nanowire formed from different diameter of parent Te nanowire. The PbTe on the thinner wires forms beaded structures with a lower pitch than on the thicker wires. (e) Bright field TEM image of the intermediate product formed at 60^{o}C after 15 min of the reaction showing the formation of a thin film over the Te nanowire. (f) EDXS elemental map for Pb and Te from the same sample. (g) High-magnification TEM image of the film region. (h) Bright field TEM image of PbTe nanowire at 60^{o}C after 3 hrs, wherein beads have been seen to form. (i) Schematic shows the variation of pitch in these nanowires with different reaction conditions.

Table of Contents Graphic: